Supplemental Material

Electronic and electrocatalytic properties of $PbTiO_3$: Unveiling the effect of strain and oxygen vacancy

L. Bendaoudi,[†] T. Ouahrani,[*,‡,¶] A. Daouli,[§] B. Rerbal,[†] R. M. Boufatah,[¶] A. Morales-García,[‖] R. Franco,[⊥] Z. Bedrane,[#] M. Badawi,[@] and D. Errandonea[*,△]

†*Laboratory of Materials Discovery, Unit of Research Materials and Renewable Energies, LEPM-URMER. Université de Tlemcen 13000 Algeria.*

‡*Ecole supérieure en sciences appliquées, ESSA-Tlemcen, BB 165 RP Bel Horizon, Tlemcen 13000, Algeria.*

¶*Laboratoire de Physique Théorique, Université de Tlemcen, Algeria.*

§*Université de Lorraine, LPCT, UMR 7019, 54506 Vandoeuvre-lés-Nancy, France*

‖*Departament de Ciéncia de Materials i Química Física & Institut de Química Teórica i Computacional (IQTCUB), Universitat de Barcelona, c/Martí i Franquès 1-11, 08028 Barcelona, Spain*

⊥*(MALTA) Consolider Team and Departamento de Química Física y Analítica, Universidad de Oviedo, E-33006 Oviedo, Spain.*

#*Laboratoire de Physique Théorique, Université de Tlemcen, Algeria.*

@*Université de Lorraine, LPCT, UMR 7019, 54506 Vandoeuvre-lès-Nancy, France*

△*Departamento de Física Aplicada - Instituto de Ciencia de Materiales, Matter at High Pressure (MALTA) Consolider Team, Universidad de Valencia, Edificio de Investigación, C/Dr. Moliner 50, Burjassot, 46100, Valencia, Spain*

E-mail: tarik.ouahrani@univ-tlemcen.dz; daniel.errandonea@uv.es

The effect of single oxygen vacancy on tetragonal $PbTiO_3$

To reduce the artificial self-image interactions imposed by periodic-boundary conditions[1] in a single-defect structure, some convergence tests were done on a number of enlarged supercells, namely 5-atoms (1×1×1), 40-atoms (2×2×2), 136-atoms (3×3×3), and 256-atoms (4×4×4). We have sampled the Brillouin zone with a k-mesh considering 12×12×11, 6×6×5, and 3×3×2, and 2×2×1 **k** meshes for supercells containing 5, 40, 136, and 256 atoms, respectively. To reveal the energetically most preferable single-defect structure, the formation energy E_f was obtained following the formula:[2]

$$E_f = E(V_O - PbTiO_3) - E(PbTiO_3) + N_O\mu_O \tag{1}$$

We have found that supercells containing 136 atoms are sufficiently large to obtain defect formation energies that converged satisfactorily (see Figure S1). This size minimizes the interaction of the vacancy with its own image in the neighboring cells. The chemical potential is used as the thermodynamic natural variable throughout all expressions for the defect formation energy and solution enthalpy. The chemical potentials of Ti, Pb, and O atoms are not independent of each other, they obey a number of restrictions based on energetic equilibrium (see Figure S6). Such conditions maintain a stable $PbTiO_3$ compound. This includes:

$$\Delta\mu_{Ti} + \Delta\mu_{Pb} + 3\Delta\mu_O = \Delta E(PbTiO_3) = -2.5060eV \tag{2}$$

where μ_{Ti}, μ_{Pb}, and μ_O are the chemical potentials of Ti, Pb, and O. $\Delta E(PbTiO_3)$ is the corresponding formation enthalpy. Other conditions that enforce the formation of single crystal compound $PbTiO_3$ with no secondary precipitate like PbO, PbO_2, Ti_2O, and Ti_3O_5.

Equation 2: $\Delta\mu_{Ti} + 2\Delta\mu_{Pb} \geq -2.5060\text{eV}$

Equation 3: $-0.333\Delta\mu_{Ti} + 0.666\Delta\mu_{Pb} \leq -0.2267\text{eV}$

Equation 4: $-1.333\Delta\mu_{Ti} + 1.666\Delta\mu_{Pb} \leq 1.8933\text{eV}$

Equation 5: $-0.666\Delta\mu_{Ti} + 0.333\Delta\mu_{Pb} \leq 0.3707\text{eV}$

Equation 6: $1.333\Delta\mu_{Ti} - 1.666\Delta\mu_{Pb} \leq 0.7957\text{eV}$

Equation 7: $1.666\Delta\mu_{Ti} - 0.333\Delta\mu_{Pb} \leq -1.2007\text{eV}$

Equation 8: $2.666\Delta\mu_{Ti} - 0.333\Delta\mu_{Pb} \leq -0.7347\text{eV}$

Equation 9: $5.666\Delta\mu_{Ti} - 0.333\Delta\mu_{Pb} \leq -0.0817\text{eV}$

Equation 10: $3.000\Delta\mu_{Ti} + \Delta\mu_{Pb} \leq -0.0600\text{eV}$

We have studied the effect of an oxygen vacancy (V_O) in the tetragonal structure of $PbTiO_3$. This single vacancy could play the role of an intrinsic defect, having critical impacts on the evolution of the physical properties. The aim of this section is to analyze the effect of the incorporation of oxygen vacancies on the exciton binding energy. Compared to the case displayed in Figure S5, the incorporation of V_O in our structure yields a decrease o the band gap. This is because the oxygen vacancy is singly ionized[3] and thus affects the transport properties of $PbTiO_3$. The calculation of the formation gives energy a value $E_f = -0.947$ eV/atom, in good agreement with the value of -0.97 eV/atom found in Ref.[4] where $E(V_O - PbTiO_3)$ and $E(PbTiO_3)$ are the total energies of defective and perfect structures, respectively. μ_0 is the atomic chemical potential of oxygen, and N_0 is the number of V_O in the cell. According to the PDOS plot of V_O-$PbTiO_3$ (see Figure S9), We can see a weak shift of Ti $3d$ orbital towards the Fermi level. This can be attributed to the fact that a change of electronic configuration from $3d^0$ to $3d^2$ occurs with localized states in the band gap. Correspondingly, the valence state of the Ti ion is expected to change from +4 to +2. This is because the Ti ion accepts two electrons from the oxygen vacancy. According to the result summarized in Table S1, the calculation of exciton-binding energy for the V_O structure is found to be very moderate, $E_b = 53$ meV, in good agreement with most organic-inorganic

metal halide perovskites.[5]

The hydrogen adsorption Gibbs free energy

In this study, the solvation effect is not taken into account due to the slight influence on the properties of HER. The hydrogen adsorption Gibbs free energy (ΔG_H) was calculated as follow:[2]

$$\Delta G_{H^*} = \Delta E^{H^*} - T\Delta S + \Delta E^{ZPE} \tag{3}$$

where $T\Delta S$ is the entropy difference between adsorbed H* and H_2 in gas phase at 298.15 K, and ΔE^{H^*} is the differential hydrogen adsorption energy

$$\Delta G_{H^*} = E^{PbTiO_3@H} - E^{PbTiO_3} - \frac{1}{2}E(H_2) \tag{4}$$

with $E^{PbTiO_3@H}$, E^{PbTiO_3} and $\frac{1}{2}E(H_2)$ representing the total energies with one hydrogen atom adsorbed on the surface, the energy of the pristine surface and H_2 molecule, respectively. ΔE^{ZPE} is the difference in zero-point energy between adsorbed H^* and molecular H_2 in the gas phase, which could be calculated as

$$\Delta E^{ZPE} = \Delta E^{ZPE}(H*) - \frac{1}{2}\Delta E^{ZPE}(H_2) \tag{5}$$

$E^{ZPE}(H*)$ being the zero-point energy of one adsorbed H^* on the catalyst obtained by $\frac{1}{2}h\nu$ without the contributions of the catalyst, and $E^{ZPE}(H_2)$ is the zero-point energy of the molecular H_2 in gas phase.

Table S1 Calculated band gap of $PbTiO_3$ using GGA + U, GGA + U + SOC, and G_0W_0. The results are compared to previous theoretical and experimental results. The table also contains the effective masses of the holes ($m_h^*(m_0)$) and electrons ($m_e^*(m_0)$), the recombination rate (m_h^*/m_e^*), and the exciton binding energy (E_b) (meV). The values ^{WM} and ^{BSE} correspond to those calculated using the two-band Wannier–Mott and quasi-particle-BSE correction model. The macroscopic dielectric function ϵ_∞ has been computed within the standard random-phase approximation (RPA), and the effective masses of carriers have been extracted from band structures of the Wannier function. (0%) and (±5%) correspond respectively to pristine and stained structures. The effective masses, the macroscopic dielectric function ϵ_∞ and the exciton binding energy (E_b) are calculated with the G_0W_0 approach

.

	E_g(eV)	$m_h^*(m_0)$	$m_e^*(m_0)$	m_h^*/m_e^*	ϵ_∞	E_b(meV)
(0%)	2.95	1.19^a, 0.87^b	2.07^c, $1.68^{\,d}$	0.46	6.99	$185^{WM}/172^{BSE}$
(-5%)	2.63	1.07^a, $1.25^{\,b}$	2.46^c, $1.09^{\,d}$, 73.64^f	0.045	6.44	$360^{WM}/320^{BSE}$
(+5%)	2.93	1.85^a, 1.68^b	1.63^g, 1.67^i	1.67	6.66	261^{WM}
V_O	1.30	2.25^j, 10.51^k	0.77^l, 2.70^m	3.66	18.72	53^{WM}
GGA + U + SOC (0%)	2.93	–	–	–	–	–
G_0W_0 (0%)	2.89	–	–	–	–	–
Exprt[?] (0%)	3.097	–	–	–	–	–

[a] corresponds to the X $\longrightarrow$ M direction
[b] corresponds to the X $\longrightarrow$ Γ direction
[c] corresponds to the Z $\longrightarrow$ A direction
[d] corresponds to the Z $\longrightarrow$ R direction
[f] corresponds to the Z $\longrightarrow$ Γ direction
[g] corresponds to the Γ $\longrightarrow$ X direction
[i] corresponds to the Γ $\longrightarrow$ M direction
[j] corresponds to the A $\longrightarrow$ Z direction
[k] corresponds to the A $\longrightarrow$ R direction
[l] corresponds to the M $\longrightarrow$ X direction
[m] corresponds to the A $\longrightarrow$ Γ direction

Table S2 Energy adsorption of the selected tested active sites, the number corresponding to the case plotted in Figure S4.

case	E_{ads} (eV)
(1)	-0.2003
(2)	-0.7456
(3)	-1.7203
(4)	-0.9364
(5)	-1.3439
(6)	-0.1618

Table S3 Energy adsorption and HER values of the pristine, structure under compression, tensile, and oxygen vacancy defective structures

case	E_{ads} (eV)	HER (eV)
Pristine (0%)	-1.7281	-1.48
compression (-5%)	-2.3166	-2.01
tensile (+5%)	-1.9181	-1.67
V_O	-0.2508	-0.03

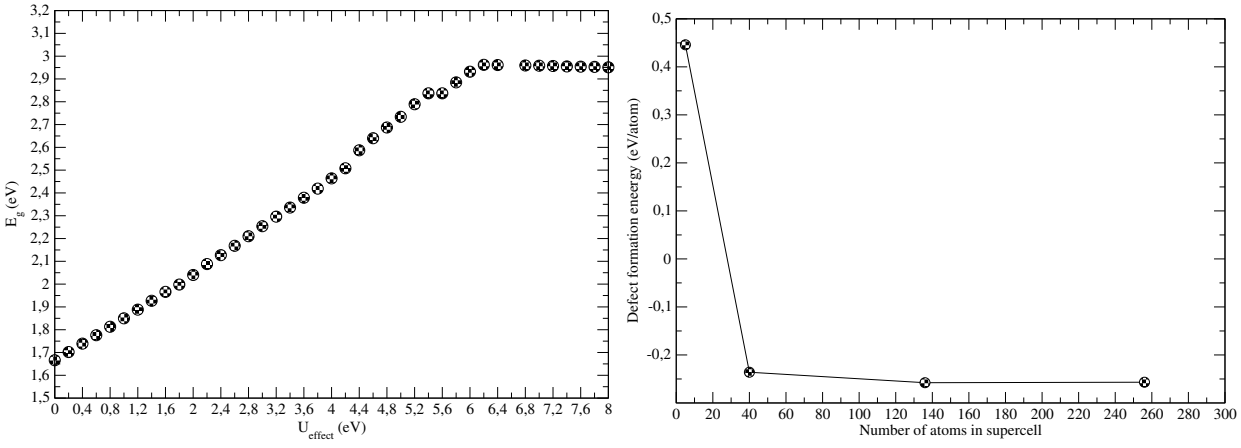

Figure S1 (Color online) Left panel: the optimization of Hubbard correction $U_{effect=U-J}$ as a function of band gap E_g. Right panel: Ab initio calculations of the single-site defect formation energies of oxygen vacancy against the size of the supercell.

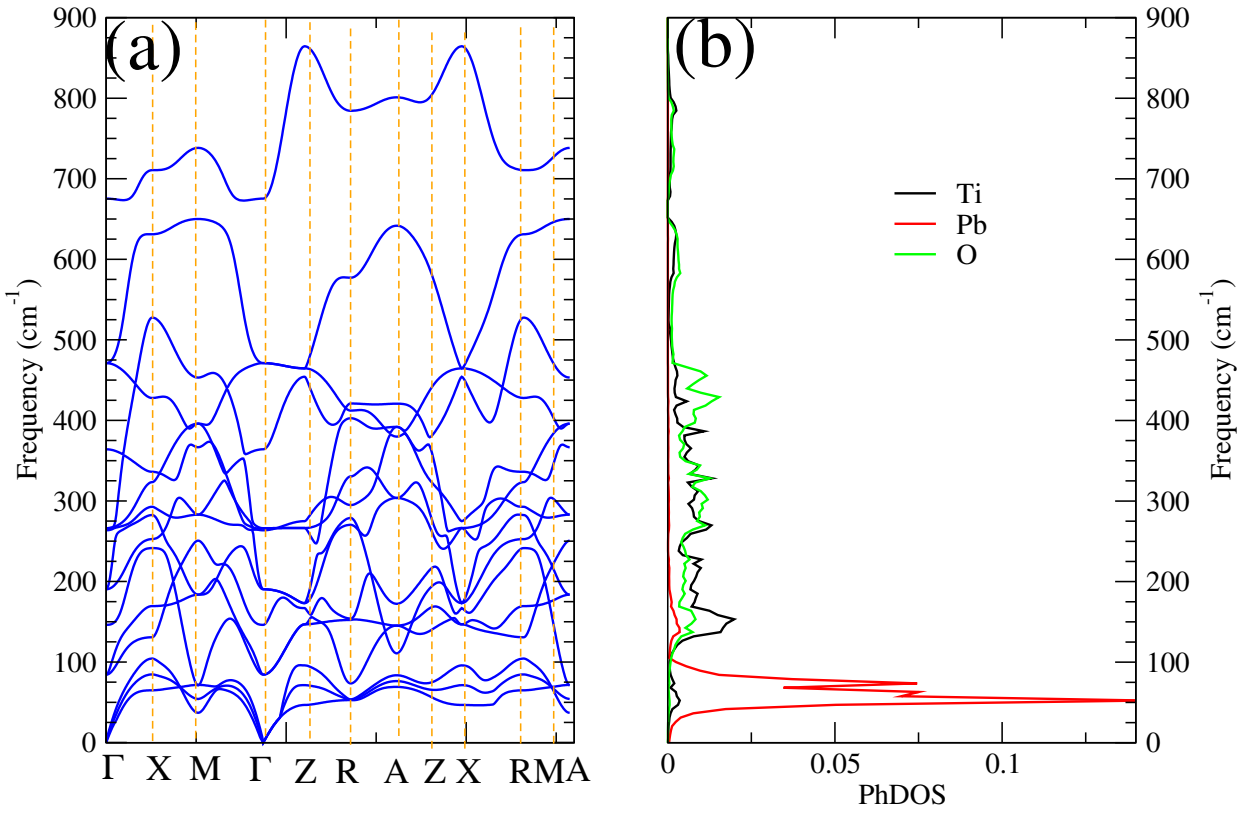

Figure S2 (Color online) (a) Calculated Phonon dispersion and (b) Calculated phonon density of states (PhDOS).

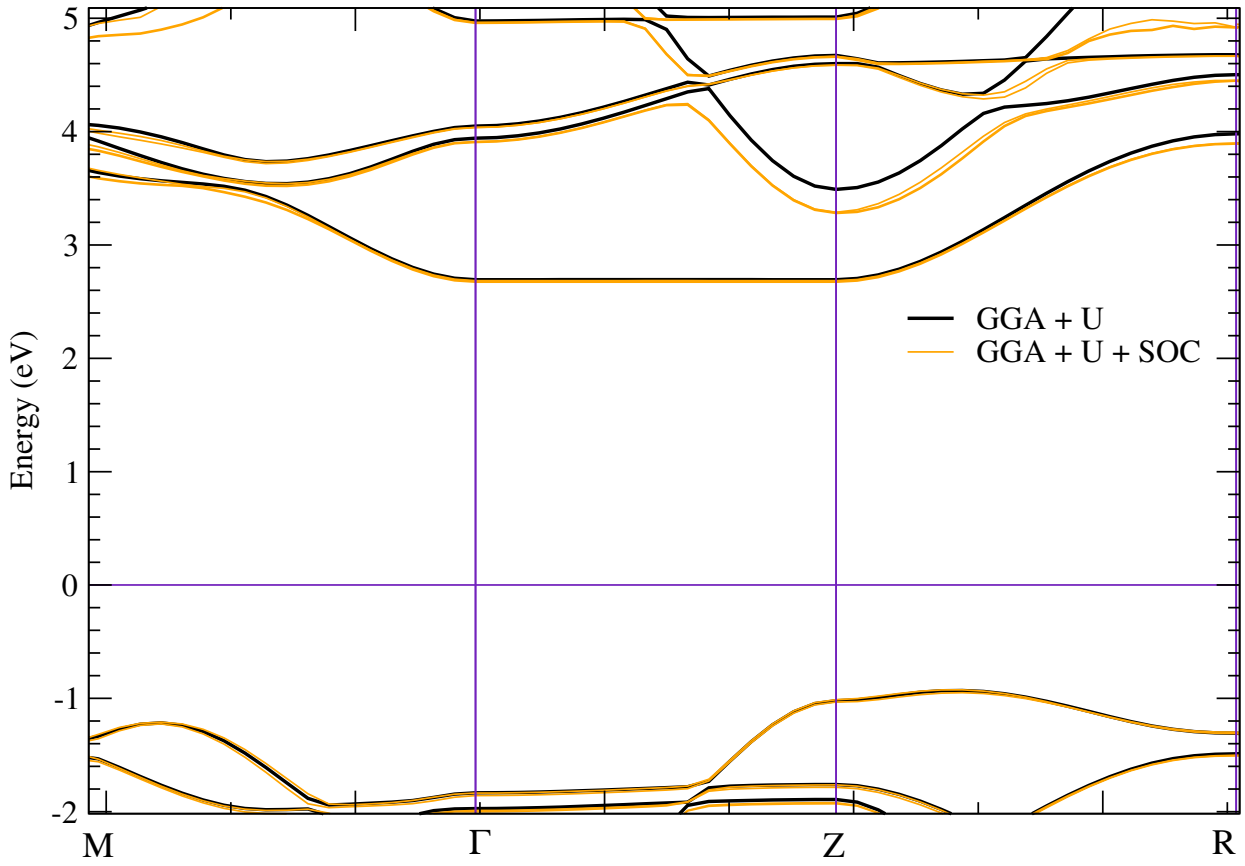

Figure S3 (Color online) a Zoom on the Band structure calculation along the $M \longrightarrow \Gamma \longrightarrow Z \longrightarrow R$ directions at GGA + U and GGA + U + SOC levels

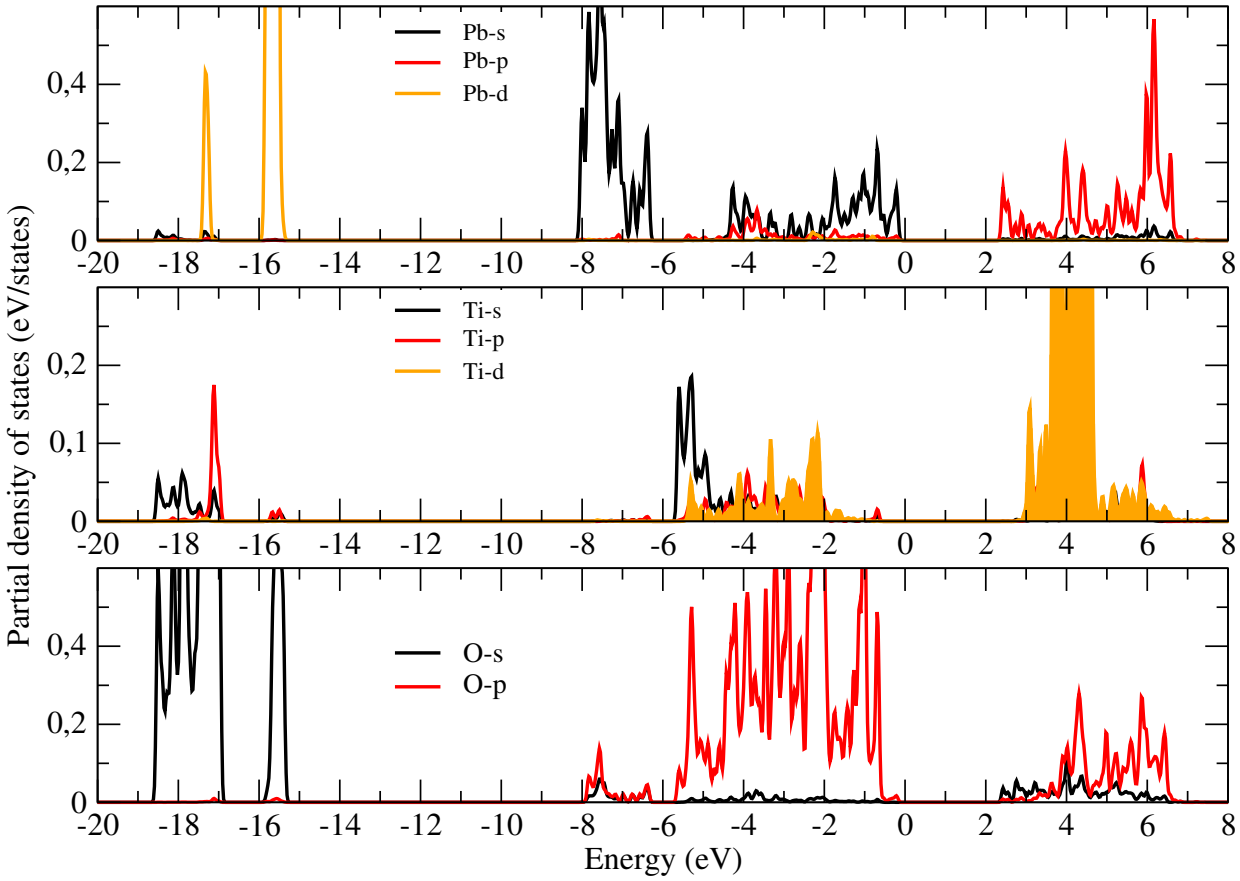

Figure S4 (Color online) Projected densities of states (PDOS) of pristine $PbTiO_3$ at GGA + U.

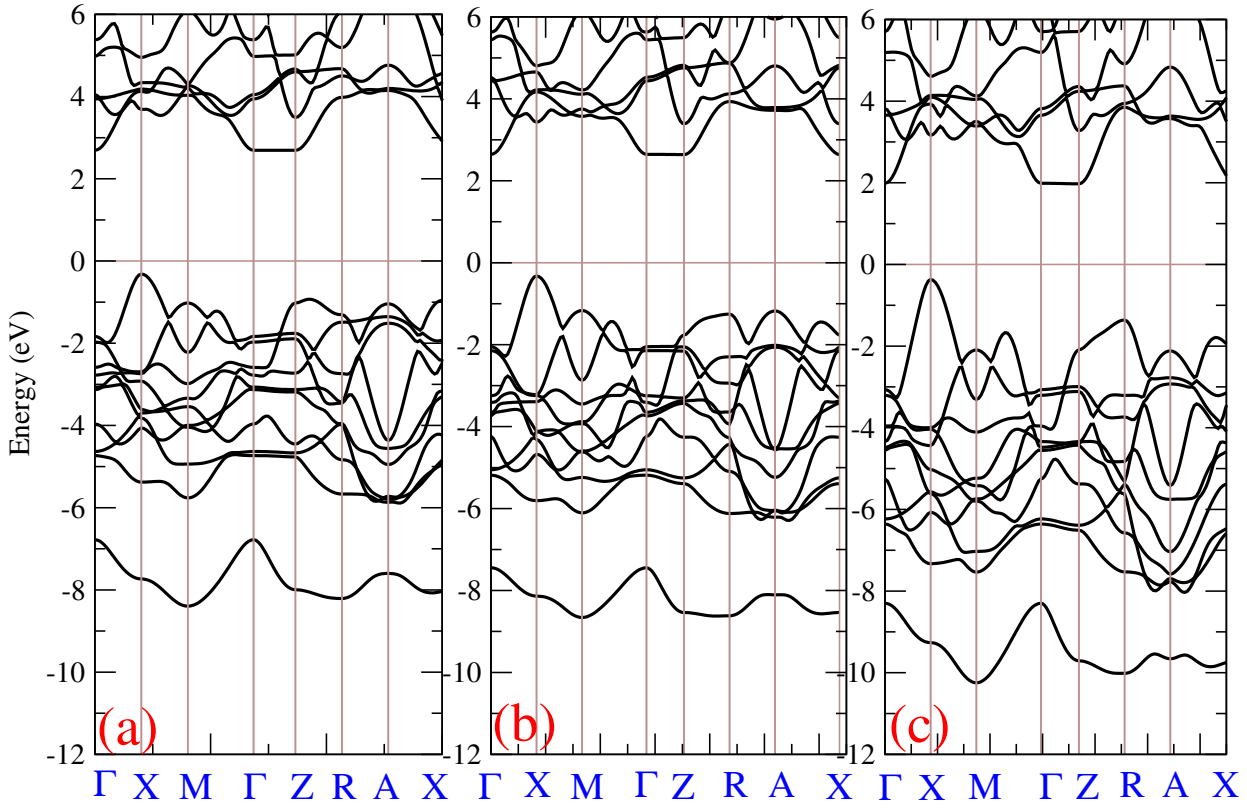

Figure S5 (Color online) band structure evolution of strained structures for (a) 0%, (b) -5%, and (c) -7%, at GGA + U level. (0%) correspond to pristine and (-5%) and (-7%) to stained structures.

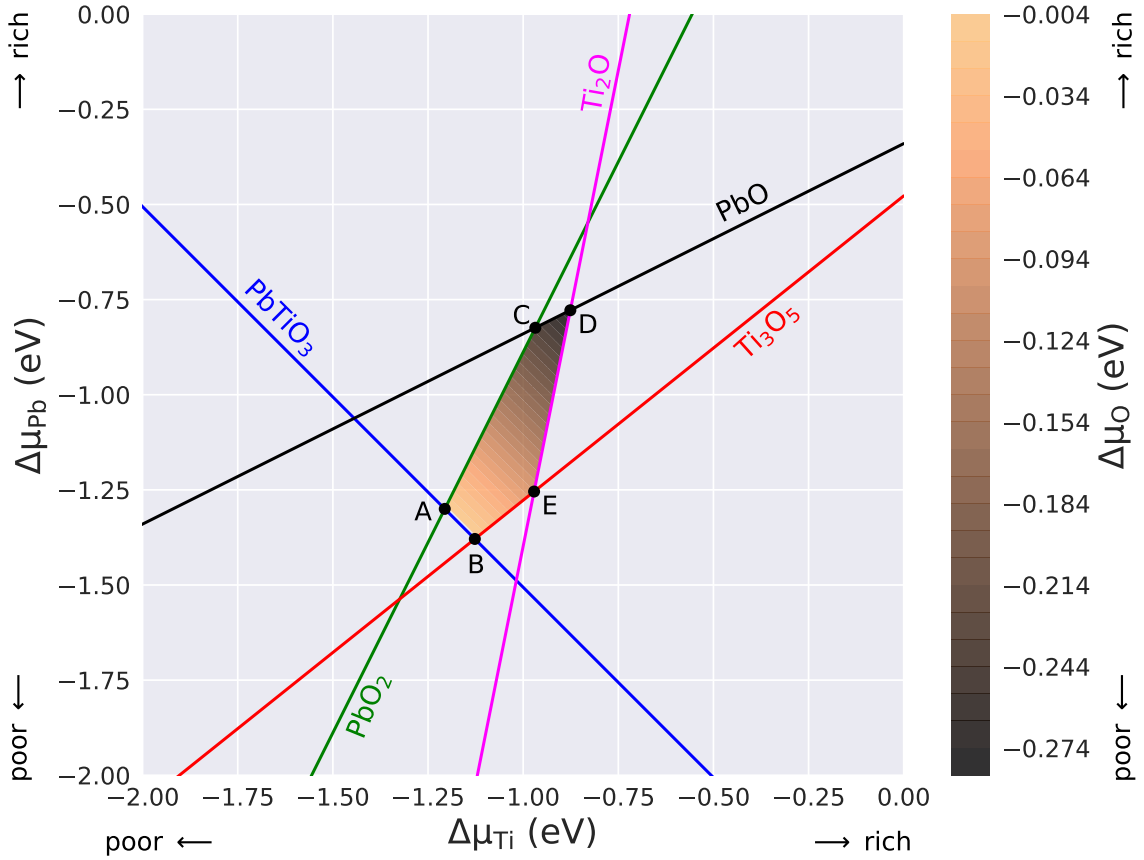

Figure S6 (Color online) Chemical potential phase diagram showing the region of stability of defective $PbTiO_3$. We show the variation in $\Delta\mu_Ti$, as a function of $\Delta\mu_Pb$ and $\Delta\mu_O$ within the stability region. Color lines are the limits imposed by competing phases. A, B, C, D, and E delimit the stability area.

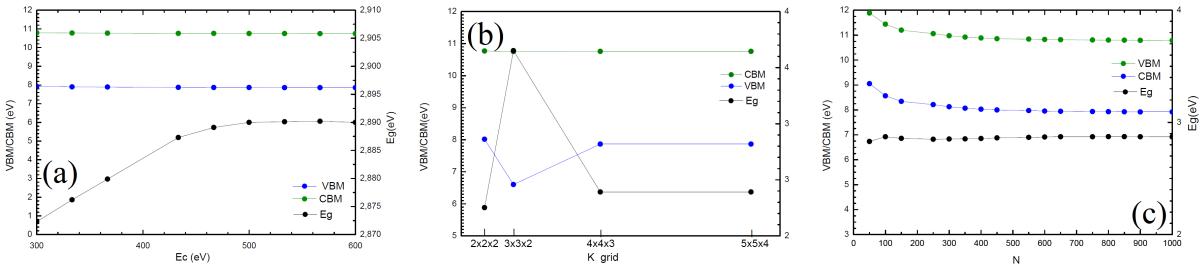

Figure S7 (Color online) Convergence of the band energy and band gap of $PbTiO_3$ with respect to (a) the energy cutoff of the response function E_ϵ at Γ Points of GW calculations, (b) k grid and (c) the number of empty states N. The convergence behaviour is insensitive for k mesh $4 \times 4 \times 3$ and N= 800 and E_ϵ=600 eV

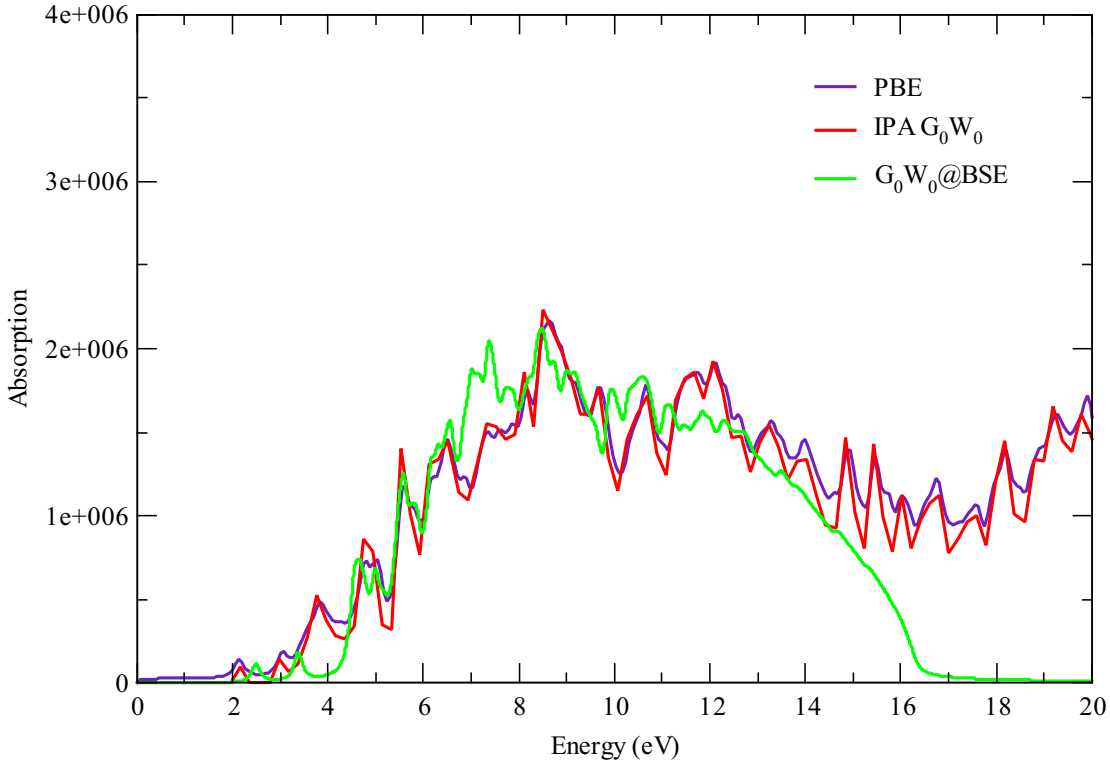

Figure S8 (Color online) The calculated absorption spectrum within PBE, IPA@GGA + U, and GW@BSE approaches.

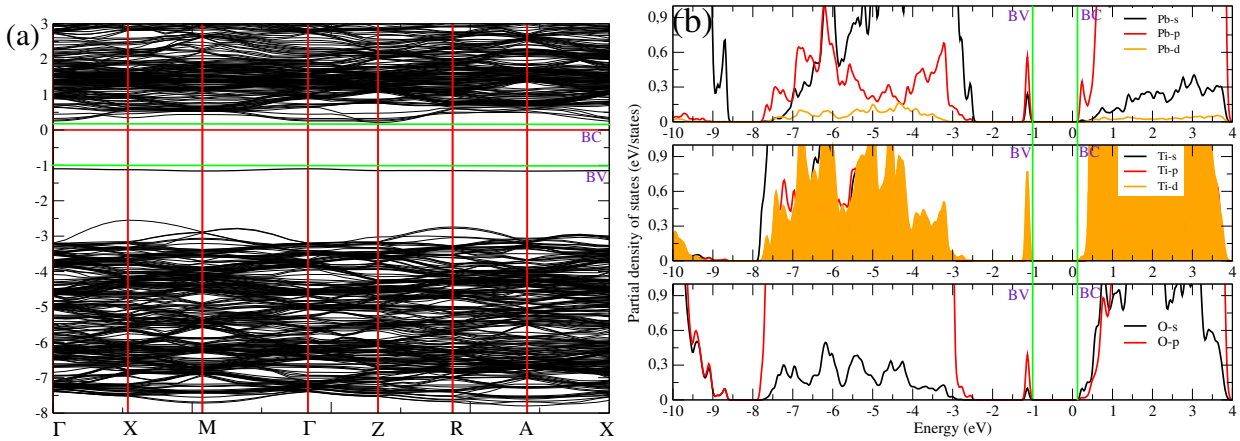

Figure S9 (Color online) (a) Band structure and (b) PDOS of the 136-atoms (3×3×3) V_O-$PbTiO_3$ structure at the GGA + U level.

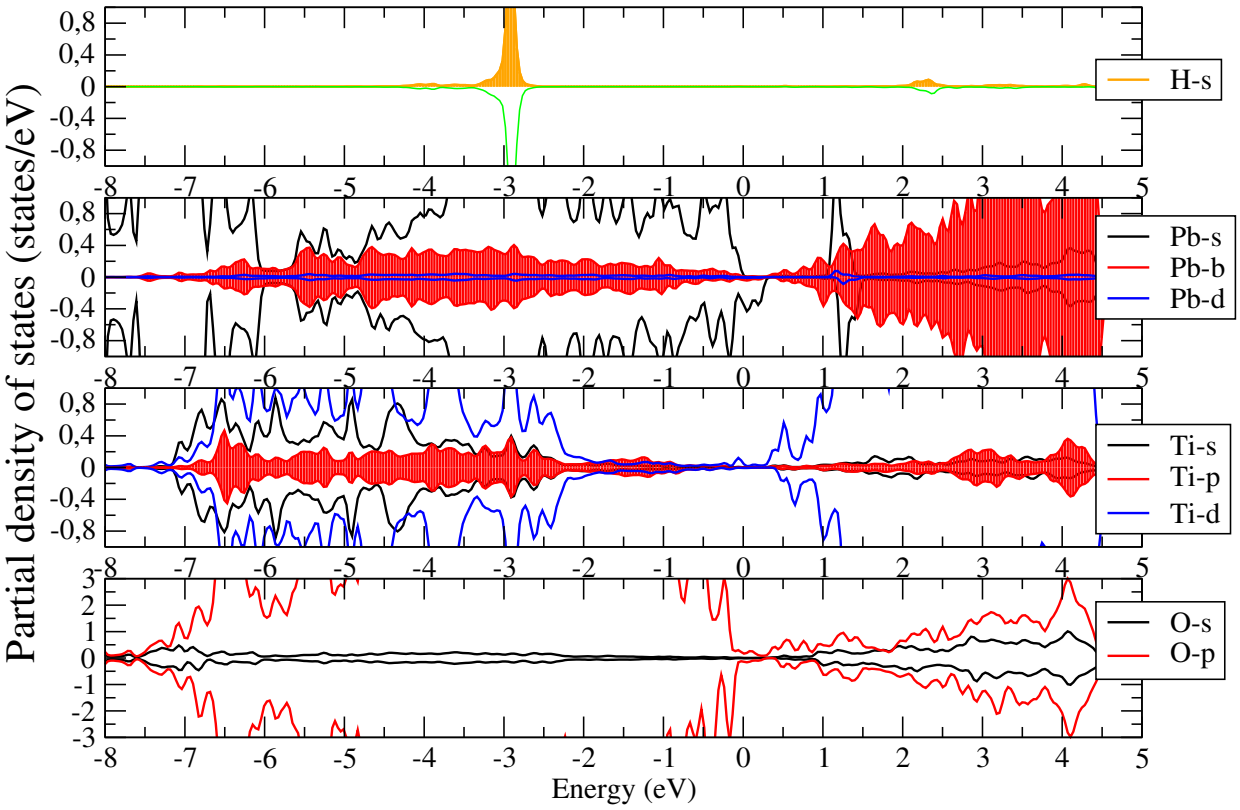

Figure S10 (Color online) Projected densities of states (PDOS) of the strained compressive (-5%) structure of $PbTiO_3$ compound at GGA + U level.

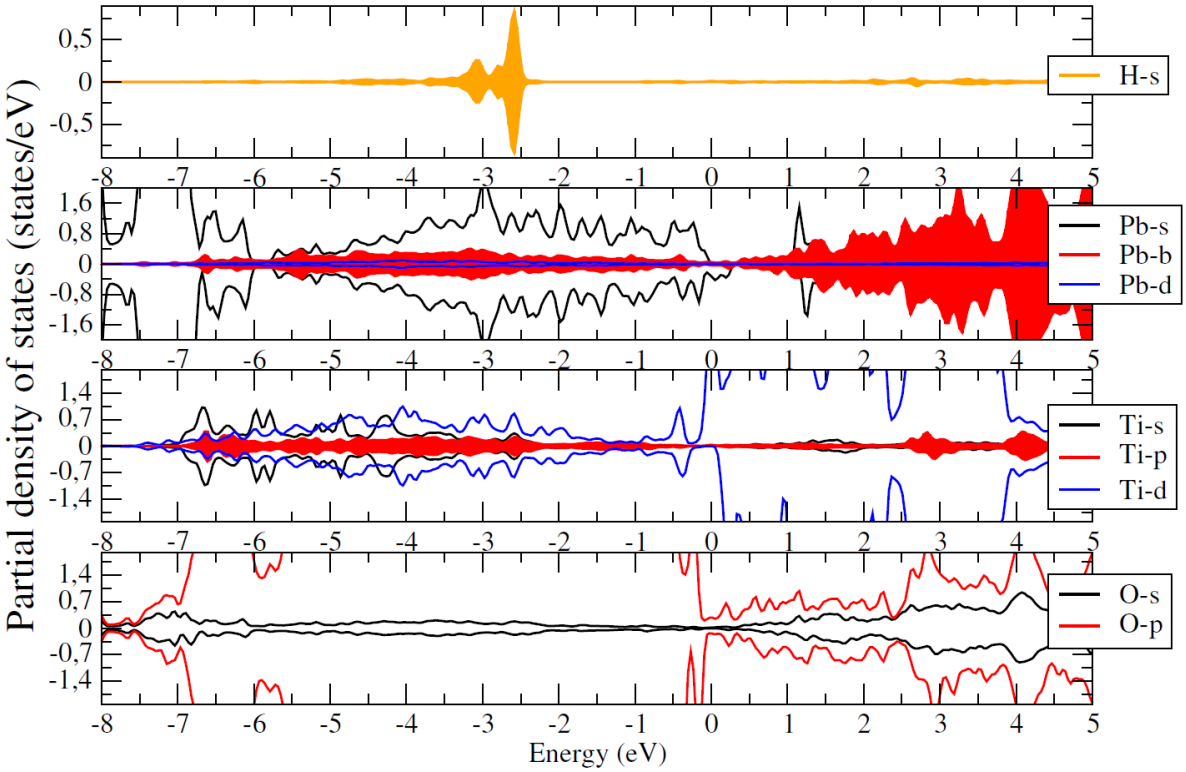

Figure S11 (Color online) Projected densities of states (PDOS) of the defective VO slab structure of $PbTiO_3$@H compound at the GGA + U level.

References

(1) J. Dabrowski and G. Kissinger, Supercell-size convergence of formation energies and gap levels of vacancy complexes in crystalline silicon in density functional theory calculations Phys. Rev.B **92**, 144104 (2015)

(2) T. Ouahrani, R.M. Boufatah, M. Benaissa, Á. Morales-García, M. Badawi, D. Errandonea, Effect of intrinsic point defects on the catalytic and electronic properties of single layer: Ab initio calculations Phys. Rev. Materials **7**, 025403 (2023).

(3) W. Gong, H. Yun, Y.B. Ning, J.E. Greedan, W.R. Datars, C.V.J. Stager, Oxygen-Deficient $SrTiO_3$-x, x = 0.28, 0.17, and 0.08. Crystal Growth, Crystal Structure, Magnetic, and Transport Properties, J. Solid State Chem. 90(1991), 320-330. https://doi.org/10.1016/0022-4596(91)90149-C

(4) Q. Yang, J. X. Cao, Y.C. Zhou, Y. Zhang, Y. Ma, X.J. Lou, Tunable oxygen vacancy configuration by strain engineering in perovskite ferroelectrics from first-principles study. Appl. Phys. Lett. 103(2013), 142911. https://doi.org/10.1063/1.4824215

(5) T. C. Sum, S. Chen, G. Xing, X. Liu, B. Wu, Energetics and dynamics in organic-inorganic halide perovskite photovoltaics and light emitters Nanotechnology, 26(2015), 34. https://doi.org/10.1088/0957-4484/26/34/342001